


A Functional Substitution in the L-Aromatic Amino Acid Decarboxylase Enzyme Worsens Somatic Symptoms via a Serotonergic Pathway

Samar Khoury, PhD ¹, Marjo H. Piltonen, PhD,¹ Anh-Tien Ton, MSc,² Tiffany Cole, BSc,³ Alexander Samoshkin, PhD,^{1,4} Shad B. Smith, PhD,⁵ Inna Belfer, MD, PhD,⁶ Gary D. Slade, BDSc, PhD,⁷ Roger B. Fillingim, PhD,⁸ Joel D. Greenspan, PhD,⁹ Richard Ohrbach, DDS, PhD,¹⁰ William Maixner, DDS, PhD,⁵ G. Gregory Neely, PhD,³ Adrian W. R. Serohijos, PhD,² and Luda Diatchenko, MD, PhD¹

Objective: Heightened somatic symptoms are reported by a wide range of patients with chronic pain and have been associated with emotional distress and physical dysfunction. Despite their clinical significance, molecular mechanisms leading to their manifestation are not understood.

Methods: We used an association study design based on a curated list of 3,295 single nucleotide polymorphisms mapped to 358 genes to test somatic symptoms reporting using the Pennebaker Inventory of Limbic Languidness questionnaire from a case-control cohort of orofacial pain ($n = 1,607$). A replication meta-analysis of 3 independent cohorts ($n = 3,189$) was followed by functional validation, including *in silico* molecular dynamics, *in vitro* enzyme assays, and measures of serotonin (5-HT) plasma concentration.

Results: An association with the T allele of rs11575542 coding for an arginine to glutamine substitution in the L-aromatic amino acid decarboxylase (AADC) enzyme was replicated in a meta-analysis of 3 independent cohorts. In a combined meta-analysis of all cohorts, this association reached $p = 6.43 \times 10^{-8}$. *In silico* studies demonstrated that this substitution dramatically reduces the conformational dynamics of AADC, potentially lowering its binding capacity to a cofactor. *In vitro* enzymatic assays showed that this substitution reduces the maximum kinetic velocity of AADC, hence lowering 5-HT levels. Finally, plasma samples from 90 subjects showed correlation between low 5-HT levels and heightened somatic symptoms.

Interpretation: Using functional genomics approaches, we identified a polymorphism in the AADC enzyme that contributes to somatic symptoms through reduced levels of 5-HT. Our findings suggest a molecular mechanism underlying the pathophysiology of somatic symptoms and opens up new treatment options targeting the serotonergic system.

ANN NEUROL 2019;86:168–180

View this article online at wileyonlinelibrary.com. DOI: 10.1002/ana.25521

Received Feb 28, 2019, and in revised form May 10, 2019. Accepted for publication Jun 2, 2019.

Address correspondence to Dr Diatchenko, Canada Excellence Research Chair in Human Pain Genetics, Department of Anesthesia, Schools of Medicine and Dentistry, McGill University, Genome Building, Room 2201, 740 Dr Penfield Avenue, Montreal, Quebec, Canada H3A 0G1.

E-mail: luda.diatchenko@mcgill.ca

From the ¹Alan Edwards Centre for Research on Pain, McGill University, Montreal, Quebec, Canada; ²Department of Biochemistry, Robert Cedergren Centre on Bioinformatics and Genomics, University of Montreal, Montreal, Quebec, Canada; ³Dr John and Anne Chong Laboratory for Functional Genomics, Charles Perkins Centre and School of Life and Environmental Sciences, University of Sydney, Sydney, New South Wales, Australia; ⁴School of Clinical Medicine, University of Cambridge, Cambridge, United Kingdom; ⁵Department of Anesthesia, Center for Translational Pain Medicine, Duke University Medical Center, Durham, NC; ⁶National Center for Complementary and Integrative Health, National Institutes of Health, Bethesda, MD; ⁷Department of Dental Ecology, School of Dentistry, University of North Carolina Chapel Hill, Chapel Hill, NC; ⁸University of Florida Pain Research and Intervention Center of Excellence, College of Dentistry, University of Florida, Gainesville, FL; ⁹Department of Neural and Pain Sciences, Brotman Facial Pain Clinic, School of Dentistry, University of Maryland, Baltimore, MD; and ¹⁰Department of Oral Diagnostic Services, University at Buffalo, Buffalo, NY

Additional supporting information can be found in the online version of this article.

A large spectrum of phenotypes encompasses the reporting of physical symptoms. The most severe manifestation consists of the somatoform disorder defined in the *Diagnostic and Statistical Manual of Mental Disorders, Fifth Edition*.¹ On the less severe end of the spectrum, the experience of multiple physical symptoms involving more than 1 bodily system for which no clear physical cause can be identified has many names,^{2–5} of which somatic awareness may be the most descriptive. Somatic awareness has been associated with both emotional distress and physical dysfunction.^{6–8} High reports of somatic awareness show strong association with a number of pain conditions including fibromyalgia, rheumatoid arthritis, and temporomandibular disorders (TMD).^{9–12} Self-reported somatic symptoms are elevated in TMD patients and are proportional to orofacial pain disability and duration.⁶ Measures of somatic awareness showed both the highest hazard ratio for predicting TMD onset¹³ and the highest odds ratios for association with chronic TMD.¹⁴ One assessment tool for quantifying somatic awareness is the Pennebaker Inventory of Limbic Languidness (PILL) questionnaire, which captures, as a global score, the frequency of occurrence of 54 common physical symptoms.¹⁴ The assessed items describe poor physical wellbeing in multiple organ systems such as gastrointestinal, cardiac, neurological, and musculoskeletal. The diversity of the symptoms captured by the PILL questionnaire characterizes somatic awareness.

Despite the relatively wide use of somatic symptom questionnaires and the importance of the related phenotypes in a range of pain conditions, our understanding of its neurobiology and molecular pathophysiology is still rudimentary. In this study, we aimed to identify genetic polymorphisms associated with somatic symptoms captured by the PILL questionnaire, and using these findings and complementary functional genomics approaches, we sought to understand the molecular mechanisms underlying the report of somatic symptoms.

Subjects and Methods

Discovery Cohort

Participants were selected from the Orofacial Pain: Prospective Evaluation and Risk Assessment (OPPERA) baseline case-control cohort, which is described in detail elsewhere.¹⁵ In brief, the OPPERA cohort is a large population-based study designed to identify the psychological and physiological risk factors, clinical characteristics, and associated genetic mechanisms that influence the development of TMD and related phenotypes. Individuals aged 18 to 44 years were recruited from 4 demographically diverse US locations (Baltimore, MD; Buffalo, NY; Chapel Hill, NC; Gainesville, FL). The discovery cohort was composed of 58.7% females, mean age \pm standard deviation 27.2 ± 7.8 , and the reported races were 55.3% non-Hispanic white, 28% African American, 6.2% Hispanic, and 10.5% other. OPPERA enrolled a total of 3,263 controls and 185 examiner-

classified chronic TMD patients. As previously published regarding the genetics of TMD within OPPERA,¹⁶ 185 TMD cases and a random selection of 50% of the OPPERA sample ($n = 1,634$) were used as a discovery cohort. The other 50% can be later used for replication. Participants were excluded if they presented major medical and psychiatric conditions that have required hospitalization, including depression.¹⁷ Medications were assessed in this cohort, including antidepressants such as selective serotonin reuptake inhibitors (SSRIs). All participants provided informed, signed consent, and the study was approved by institutional review boards at each of the 4 study sites and at McGill University.

Pennebaker Inventory of Limbic Languidness

All participants completed the PILL questionnaire via paper or electronically. PILL assesses the frequencies of occurrence of 54 common health complaints (eg, coughs, headaches, sore joints/muscles, nausea, congested nose, abdominal pain). For each symptom, frequencies are endorsed as 1 (never/almost never), 2 (less than 3 or 4 times per year), 3 (every month or so), 4 (every week), or 5 (more than once per week). The PILL global score is the sum of the frequency score reported for each of the 54 symptoms, ranging from 54 to 270.¹⁴ The PILL global score is related to somatic awareness or the general tendency to endorse physical symptoms. The PILL questionnaire has been shown to have high internal consistency (Cronbach $\alpha = 0.88$) and acceptable test-retest reliability over 2 months (0.79).^{14,18} In terms of the validity of the PILL questionnaire in the context of other somatic awareness questionnaires, OPPERA also assessed somatic awareness using the Symptom Checklist-90 (SCL-90) somatization scale. The PILL and SCL-90 somatizations are highly correlated with each other (PILL vs SCL-90 somatization: $\rho = 0.707$; $p < 0.0001$). When possible, missing global scores were imputed using a maximum likelihood estimate in SAS PROC MI (SAS Institute, Cary, NC). Overall, the PILL global score was available for 184 TMD cases and 1,633 noncase controls for OPPERA. The PILL global score represents the primary outcome in this study.

Genotyping

Whole blood was collected from consented participants, and genomic DNA was extracted and purified using QIAGEN (Hilden, Germany) extraction kits. DNA samples were genotyped using the Algenomics (Chapel Hill, NC) Pain Research Panel, a dedicated chip-based platform utilizing the AFFYMETRIX MegAllele technology.¹⁶ The Pain Panel assesses 3,295 single nucleotide polymorphisms (SNPs) representing 358 genes known to be involved in systems relevant to pain phenotypes and have been selected by 4 independent experts. Pathways assessed by the Pain Panel represent 1 or more of 3 broad domains and include genes that (1) mediate the transmission of pain signals by sensory nerve fibers and by central nervous system neural pathways that mediate the perception of pain, (2) mediate peripheral and central inflammatory responses to tissue injury or psychological stress, and (3) influence mood and affective states associated with chronic pain conditions. The Pain Panel also includes genes that influence the pharmacokinetics and dynamics of analgesic compounds and includes ancestry-informative markers. Within each

gene, SNPs were prioritized for inclusion based on known or potential functionality. Other SNPs were selected as representative markers of regions with high linkage disequilibrium.

Quality-control procedures were applied using PLINK version 1.07.¹⁹ SNPs with call rate <0.95 ($n = 170$), concordance rate of <0.99 ($n = 58$), minor allelic frequency of <1% ($n = 101$), and a Hardy-Weinberg equilibrium $p < 1 \times 10^{-5}$ ($n = 42$) were removed. The final cleaned number of SNPs used for the analysis was 2,924. Following sample quality control, OPPERA samples were dropped due to call rate <0.95 ($n = 38$), cryptic relatedness with a π -hat of 0.185 ($n = 84$), mismatch between self-reported race and sex ($n = 29$), and duplicate genotypes ($n = 36$). The final clean samples that passed quality check for genotyping included 165 TMD cases and 1,442 healthy controls, for a total of 1,607.

Replication Cohorts

Three independent cohorts were used to replicate the findings from the discovery OPPERA cohort. The first replication cohort consisted of an independent chronic TMD study. This TMD case-control study was collected from the community surrounding University of North Carolina-Chapel Hill and enrolled non-Hispanic white females aged 18 to 60 years comprised of 199 chronic TMD cases and 201 noncase controls. Details of this cohort have been described elsewhere.²⁰ To increase power, the remaining half ($n = 1,629$) of the controls in the original OPPERA cohort were added. This cohort was also genotyped using the Algynomics Pain Research Panel and was subjected to the same quality control procedures as the discovery cohort. The final sample size consisted of 184 TMD cases and 1,599 noncase controls for a total of 1,783. The same quality-control procedures as the discovery cohort were applied.

The second replication cohort was derived from the Post-Mastectomy Pain Syndrome (PMPS) study. This cohort ($n = 1,200$) was recruited from the Comprehensive Breast Cancer Program's registry of breast cancer patients undergoing total or partial mastectomy at Magee Women's Hospital of University of Pittsburgh Medical Center. University of Pittsburgh Institutional Review Board approval was obtained prior to all data collection, and all patients gave informed consent before participation in the study. Patients completed the PILL questionnaires a mean of 38.3 ± 35.4 months (range, 2 months-10 years) after surgery. Full cohort description was reported elsewhere.²¹ DNA was extracted from lymph node tissue, blood, or saliva. A total of 665 subjects were genotyped using the UK Biobank Axiom platform by the Genome Center at McGill University. The same quality-control procedures as the discovery cohort were applied.

The third replication cohort was the Complex Persistent Pain Conditions (CPPC): Unique and Shared Pathways of Vulnerability cohort. It included 900 participants enrolled in a case-control study of overlapping pain conditions conducted at the University of North Carolina-Chapel Hill. Participants were aged 18 to 64 years, included both sexes (86% female), and included major ethnic and racial groups (68% non-Hispanic white). This cohort included individuals with either at least 1 of 4 index CPPCs (episodic migraine, irritable bowel syndrome,

fibromyalgia, or vulvar vestibulitis) or with none of these conditions. The questionnaire was administered to all subjects. DNA was extracted from blood, and 741 subjects were genotyped using the Axiom Precision Medicine Research Array by Genome Center at McGill University. The same quality control procedures as the discovery cohort were applied.

Genetic Analysis

Genetic analysis was done using PLINK 1.09b2.¹⁹ For the discovery cohort, a linear regression model was applied using quantitative data from the PILL global scores with TMD case status, gender, age, dummy coded recruitment site, and the first 2 eigenvectors derived from principal component analysis to account for ancestry as covariates. The analysis was also performed using log-transformed PILL global scores to account for the skewness of the data distribution. Statistical significance was set at a false discovery rate (FDR) of 5%. At this threshold, we had 71% power to detect an effect with 1% variance in the discovery cohort. The same linear model, including the same covariates, was used for the replication cohorts. The replication phase consisted of the replication of SNPs that passed FDR threshold in the discovery cohort. The statistical significance threshold for replication was determined using Bonferroni correction for the number of SNPs to be replicated.

A meta-analysis was then performed to combine the 3 replication cohorts' results using METAL²² with an inverse-variance-weighted method followed by a meta-analysis combining all cohorts. The meta-analysis of the 4 cohorts had a sample size of 4,796. With this sample size, we had 99.7% power to detect a 1% effect.

Molecular Dynamics Simulations

The *DDC* (dopa decarboxylase) gene codes for the homodimeric enzyme L-aromatic amino acid decarboxylase (AADC) that requires binding a cofactor pyridoxal 5'-phosphate (PLP) for its activity. AADC protein structures were obtained from the Research Collaboratory for Structural Bioinformatics Protein Data Bank (PDB; PDB IDs: 3RCH for the holo form, and 3RBF for the apo form).²³ The holo form refers to the catalytically active enzyme with the cofactor PLP, whereas the apo form is the enzyme without its cofactor. The R462Q substitution was introduced to both chains of the dimers with the Eris software's mutagenesis tool using the flexible backbone option.²⁴ Molecular dynamics simulations and system equilibration for the R462 and Q462 structures were performed with the GROMACS version 5.0.5 molecular simulation package,²⁵ using the GROMOS9654a7 force field.²⁶ The custom topology for the cofactor PLP peptides was constructed with PRODRG 2.5²⁷ and added to the AADC topology file. The AADC protein dimer and PLP peptide complex were centered in a cubic box. The periodic water box edges were extended at least 20Å away from the complex to allow it to move freely during the production runs. The SPC216 water model was used to solvate the system and to add water molecules to the box.²⁸ Na⁺ and Cl⁻ ions were added as necessary to have a 0 net charge in the box. Four systems of molecular dynamics simulations were performed: the holo-R462, holo-Q462, apo-R462, and apo-Q462. Each system was submitted to 5,000 steps of energy

minimization using a steepest descent method to remove initial steric clashes and assure appropriate geometry. The particle mesh Ewald algorithm²⁹ was used in all calculations to consider electrostatic interactions with grid spacing around 1Å, and van der Waals forces were considered with a cutoff distance of 1.4Å. Each system was subjected to 2 rounds of equilibration after minimization. They were first gradually heated in a canonical ensemble: amount of substance: N, volume: V, and temperature: T (NVT) from 0 to 300K over 10ps using the V-rescale coupling algorithm³⁰ with position restrains on the protein and the ligand. This was followed by an isothermal-isobaric ensemble: amount of substance: N, pressure: P, and temperature: T (NPT) equilibration of 10ps to reach the reference pressure of 1atm by using the Parrinello-Rahman coupling algorithm³¹ with isotropic coupling and with position restrains on the protein and the ligand. The LINear Constraint Solver (LINCS) algorithm was used to constrain all bonds involving hydrogen atoms.³² Due to the size of the protein and ligand complex, each system ran for 10ns molecular dynamic simulation until equilibration under the same conditions as the equilibration procedures with a time step of 2fs, without any position restrains. Computations were made on the supercomputer Briarée from the University of Montreal, managed by Calcul Quebec (Montreal, Quebec, Canada) and Compute Canada (Toronto, Ontario, Canada). Production runs requested 48 cores. The analysis for the trajectories was carried out using the standard software tools provided by the GROMACS package, and visualization was performed with VMD³³ and PyMol.

Expression of DDC Variants In Vitro

HEK293 cells were grown in T-75 flasks and then seeded on 100-mm dishes and were transfected with 4µg of vectors that carry either the major allele, referred to as pcDNA3-DDC_c, or the minor allele (T), referred to as pcDNA3-DDC_t, using 20µl of X-tremeGENE HP DNA Transfection Reagent (Roche, Basel, Switzerland). Empty pcDNA3 vector was used as a negative control. Cells were harvested 24 hours after transfection by first rinsing them with phosphate-buffered saline and then scraping them into 1.4ml of assay buffer (10mM NaH₂PO₄ pH 7.4, 1mM MgCl₂, and 1µM DTT). Cells were sonicated and then centrifuged at 5,000 × g at +4°C for 5 minutes, and the supernatant was collected to a new tube and stored at -20°C. DDC-variant transfections were repeated 5 times, but empty vector or untransfected cells were harvested only twice, as HEK293 cells did not express a measurable background AADC expression or activity.

Western Immunoblotting of Transiently Expressed DDC Variants

Protein concentrations of the lysates were first measured with Pierce BCA Protein Assay Kit (Thermo Fisher Scientific, Waltham, MA). AADC protein that resulted from vectors carrying the pcDNA3-DDC_c was defined as AADC_R for arginine, and the AADC protein that resulted from vectors carrying the pcDNA3-DDC_t was defined as AADC_Q for glutamine. A lysate volume containing 10µg of total protein was mixed with an equal volume of 2xLaemmli buffer (Bio-Rad, Hercules, CA) containing 2% β-mercaptoethanol and boiled at 95°C for 5 minutes. Proteins were separated on a NuPage

4-12% Bis-Tris precast gels (Thermo Fisher Scientific) and transferred to a polyvinylidene fluoride (PVDF) membrane (Bio-Rad) using the Transblot Turbo blotter (Bio-Rad). Membranes were blocked in 5% nonfat milk for 1 hour at room temperature, and then incubated overnight at 4°C with the primary antibody against AADC (1:1,000; rabbit polyclonal ab189101; Abcam, Cambridge, United Kingdom) or anti-β-actin (1:5,000; rabbit polyclonal ab8227; Abcam). The next day, the membranes were incubated with goat anti-rabbit immunoglobulin-G HRP polyclonal secondary antibody (1:3,000; Bio-Rad) for 1 hour at room temperature. Bands were visualized with a chemiluminescence reagent (Amersham ECL Prime Western Blotting Detection Reagent; GE Healthcare, Chicago, IL), and detected with a digital imager (Amersham Imager 600; GE Healthcare). Pixel densities of the bands were measured in an ImageQuant TL (GE Healthcare) using a user-defined background correction. AADC signals were first normalized against β-actin signals, and then against AADC_R. Only after analysis, for clarity, the brightness of the figures of immunoblots was adjusted by approximately +45 units in Adobe Photoshop CS6 (Adobe, San Jose, CA) so that no crucial information was obscured. All 5 individual transfection experiments were blotted, and lysate from the BE(2)-C neuroblastoma cell line was used as a positive control for antibody specificity.

AADC Enzymatic Activity Assay and Detection of Decarboxylation Products

The enzymatic assay for this study was adapted from the studies by Allen.³⁴ In brief, 25µl of lysate (raw for 5-HTP, 1:10 diluted in assay buffer for L-dopa) was added to 87.5µl of reaction mix and incubated for 120 minutes at +37°C in a water bath, and 12.5µl of 10× concentrated L-dopa (3,4-dihydroxy-L-phenylalanine; Sigma-Aldrich, St Louis, MO) or 5-HTP (5-hydroxy-L-tryptophan; Sigma-Aldrich) in 10mM hydrochloric acid was added as a substrate, and the reaction mix was incubated for 5 minutes. Final concentrations in the reaction mix at this point were: 0-1000µM L-dopa or 5-HTP, and 70µM pyridoxal 5'-phosphate (Sigma-Aldrich) as a cofactor in 100mM phosphate buffer pH 7.2 (L-dopa) or 7.4 (5-HTP). The reactions were then stopped by adding 12.5µl of ice-cold 4M perchloric acid and quick vortexing. The samples were left at room temperature for 10 minutes, after which they were centrifuged at 17,000 × g at +4°C for 10 minutes to precipitate proteins and cell debris. Supernatants were filtered to fresh tubes through Millex-HV syringe filters (4mm; 0.45µm PVDF; Millipore, Burlington, MA). Samples that received 10 to 1,000µM 5-HTP or 100 to 1,000µM L-dopa were diluted 1:10 before analysis to keep concentrations in the linear detection range.

Concentrations of decarboxylation reaction products, dopamine (DA), and 5-hydroxytryptamine (5-HT [serotonin]) were determined with a ultra-high performance chromatography (UHPLC) instrument (Dionex UltiMate3000 RS, Thermo Fisher Scientific) with an 8-cell coulometric array detector (CoulArray 5600A, Thermo Fisher Scientific). Samples were kept at +4°C in the autosampler, and 10µl of sample were injected for detection. The mobile phase consisting of 6.25% acetonitrile in a 0.1M phosphate solution (pH 3.0) with 1mM ethylenediaminetetraacetic acid (EDTA) and 1.5mM 1-octanesulfonic acid was pumped at

0.325ml/min. Analytes were separated in a column (Kinetex C18, 2.6 μ m, 2.1 \times 100mm; Phenomenex, Torrance, CA) that was kept at 45°C. Detector cells were set to 50 to 450mV. A standard curve for DA and 5-HT was run each time, and the sum of primary peaks was used in computing the concentrations for both analytes.

AADC activity was calculated as pmol/min/mg protein using the formula (product formed [μ M] \times V_{assay} [ml] \times 1000)/(prot. conc [mg/ml] \times V_{enzyme} [ml] \times time [min]). Protein concentrations of the lysates were the same as determined for Western blot. The final results were obtained by normalizing the activities against their relative expression levels determined by Western blot (activity/expression). To account for the variability between experiments, all values were expressed relative to AADC_R at 1,000 μ M substrate concentration (=100% activity). Results were plotted in GraphPad Prism 6.03 (GraphPad Software, San Diego, CA) and fitted with Michaelis-Menten non-linear regression curves to obtain kinetic parameters (Michaelis constant [K_m] and maximum velocity [V_{max}]).

Plasma Levels of DA and 5-HT

Plasma was extracted from whole blood of the CPPC cohort in a subset of 90 participants. Plasma was diluted 1:4 or 1:6 with cold 0.3M perchloric acid in microcentrifuge tubes. The tubes were then centrifuged at 17,000 \times g at 4°C for 15 minutes to precipitate debris and proteins. The supernatant was filtered using Millex-HV syringe filters (PVDF membrane, 0.45 μ m and 0.22 μ m; Millipore). The concentrations of 5-HT were determined with a UHPLC (Dionex UltiMate3000 RS; Thermo Fisher Scientific) combined with a coulometric array detector (CoulArray 5600A, Thermo Fisher Scientific). The concentrations of DA were below detection threshold and therefore undetectable. The mobile phase consisted of 6% acetonitrile in a 75mM phosphate solution (pH 3.0), supplemented with 25 μ M EDTA and 0.75mM 1-octanesulfonic acid. The analytes were separated from a 20 μ l injection in a Kinetex C18, 2.6 μ m, 4.6 \times 150-mm column (Phenomenex) that was kept at 40°C. The data were analyzed in the CoulArray software using primary peak areas as a measure for the amount of analyte. The detection limit was approximately 0.3nM (52pg/ml for 5-HT).

Results

Discovery Cohort OPPERA Characteristics

The discovery cohort was comprised of 58.7% females, mean age of 27.2 \pm 7.8 years, and the reported races were 55.3% non-Hispanic whites, 28% African American, 6.2% Hispanic, and 10.5% other. Recruitment was done in Florida (28.9%), followed by North Carolina (27.4%), and equally in New York and Maryland (21.4% and 22.3%, respectively). The cohort was comprised of 10.3% of TMD cases and 89.7% noncase controls (Supplementary Table 1). PILL global scores did not follow a normal distribution (Shapiro-Wilk $p < 0.0001$) with a mean score of 91.1 \pm 23.9. There was a significant mean difference in PILL global scores between TMD cases and controls (114.8 \pm 32.3 for TMD cases, 88.4 \pm 21.1

for controls, $p < 0.0001$), with TMD cases reporting more somatic symptoms. Non-Hispanic whites had the worse symptoms (mean = 95.02 \pm 23.93), followed by Hispanics (88.16 \pm 20.42) and African Americans (86.00 \pm 24.56), who had the lowest scores.

Genetic Association with PILL in OPPERA

In the discovery cohort OPPERA, genotypes of 165 TMD cases and 1,442 controls passed quality controls and were included in the analysis. There was some genomic inflation in the genetic association data ($\lambda = 1.07$). A linear model showed that 5 SNPs in 5 distinct genes passed FDR 5% (Table 1, Fig 1A). Of those SNPs, 3 were intron variants and 2 were nonsynonymous variants. To account for the skewness in the distribution of global PILL scores, we also undertook an analysis using log-transformed PILL scores as a dependent variable, and the results also show the same strength of association (Supplementary Table 2). Moreover, to make sure that the diverse ancestry in the discovery cohort is accounted for, we performed a separate analysis in non-Hispanic whites and in African Americans, followed by an inverse-variance-weighted meta-analysis. Again, the strength of the association remained very similar (see Supplementary Table 2). Furthermore, a separate analysis in controls and TMD cases only shows that the effect size is very similar, even if the association was not statistically significant in cases most likely due to small sample size (Supplementary Table 3).

Replication and Meta-Analysis

In the 3 replication cohorts (Supplementary Tables 4, 5, and 6), we sought to test the 5 SNPs from the discovery cohort and therefore set the threshold for statistical significance at $p = 1.0 \times 10^{-2}$.

In the first replication cohort, TMD case control, a total of 1,783 individuals passed genotyping quality check. From the 5 tested SNPs, only 1 SNP passed the statistical threshold for multiple comparison and was in the same direction of association as the discovery cohort, namely rs11575542 ($\beta = 6.62$, standard error [SE] = 1.65, $p = 6.27 \times 10^{-5}$) located in the *DDC* gene (Table 2). The minor allele T of rs11575542 was associated with higher PILL global scores with a minor allelic frequency of 5.05%.

In the second replication cohort, PMPS, all 5 SNPs were either genotyped or imputed. None of the tested SNPs passed the threshold for significance; however, 1 SNP, rs3020422 located in the estrogen receptor 1 gene, was nominally associated with PILL global scores ($\beta = -5.36$, SE = 2.37, $p = 0.02$; see Table 2).

In the third replication cohort, CPPC, all 5 SNPs were either genotyped or imputed. However, none of the SNPs passed the threshold for significance (see Table 2).

TABLE 1. SNPs Associated with Pennebaker Inventory of Limbic Languidness Scores in the Discovery Orofacial Pain: Prospective Evaluation and Risk Assessment Cohort

SNP	Chr	Gene	Function	EA	β (SE)	p	FDR
rs2498982	1	<i>PATJ</i>	Missense	G	3.03 (0.80)	1.60E-04	1.30%
rs3765550	9	<i>MPDZ</i>	Intron	C	3.02 (0.84)	3.27E-04	2.58%
rs1563945	8	<i>PNOC</i>	Intron	C	-3.62 (1.02)	3.70E-04	2.85%
rs11575542	7	<i>DDC</i>	Missense	T	6.45 (1.86)	5.25E-04	3.94%
rs3020422	6	<i>ESR1</i>	Intron	A	-2.87 (0.83)	5.57E-04	4.07%

Chr = chromosome; *DDC* = L-aromatic amino acid decarboxylase; EA = effect allele; *ESR1* = estrogen receptor 1; FDR = false discovery rate; *MPDZ* = multiple PDZ domain crumbs cell polarity complex component; *PATJ* = PatJ, crumbs cell polarity complex component; *PNOC* = prepronociceptin; SE = standard error; SNP = single nucleotide polymorphism.

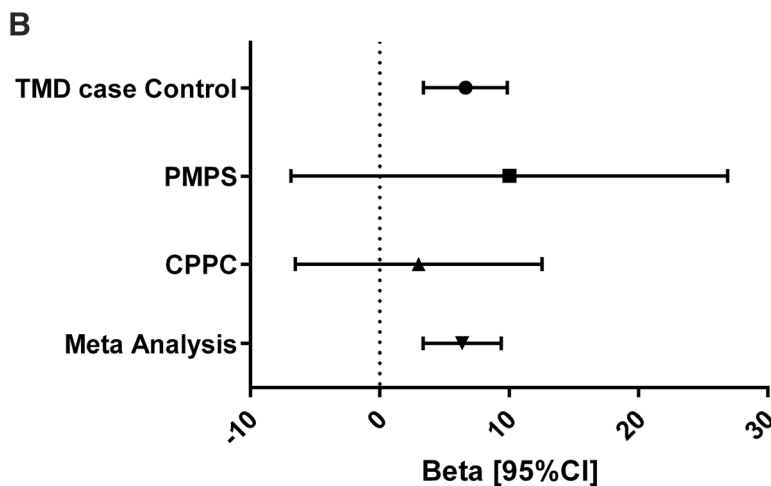
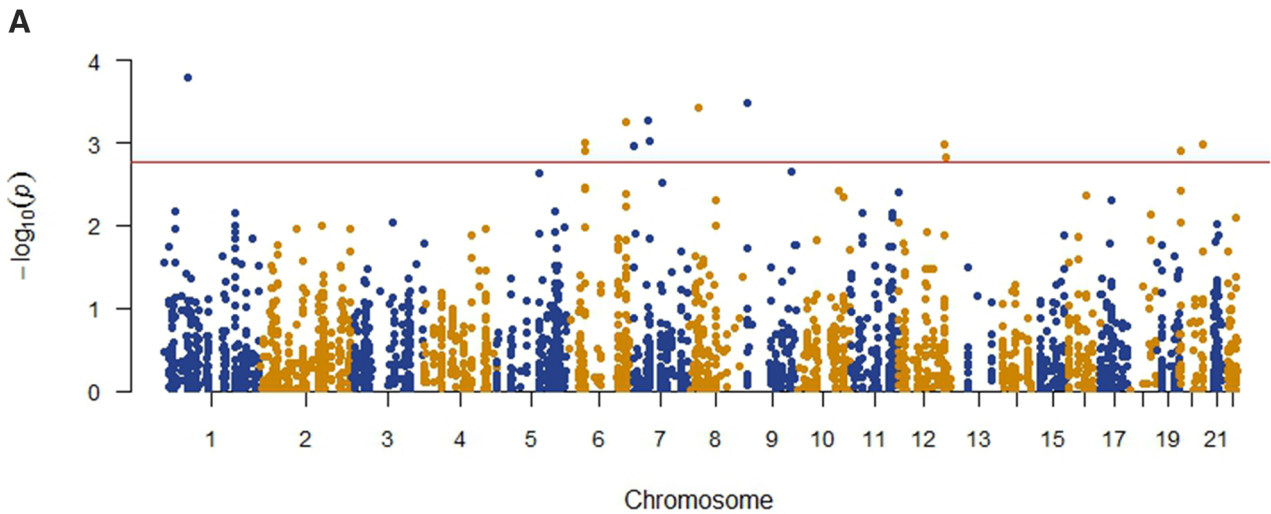


FIGURE 1: Genetic association study results of somatic symptoms (PILL global scores) in the discovery cohort and meta-analysis. (A) Manhattan plot: the x-axis shows chromosomes and the y-axis shows $-\log_{10} p$ value of associations. The threshold line represents FDR 5%. (B) Forest plots: forest plot of effect sizes with 95% confidence interval for each replication study as well as for the fixed-effect meta-analysis for rs11575542. CI = confidence interval; CPPC = complex persistent pain conditions cohort; PILL = Pennebaker Inventory of Limbic Languidness; PMPS = postmastectomy pain syndrome cohort; TMD = temporomandibular disorders case-control cohort. [Color figure can be viewed at www.annalsofneurology.org]

In an inverse-variance-weighted meta-analysis combining the 3 replication cohorts, for a total sample size of 3,189, only rs11575542 (effect allele: T; $\beta = 6.37$, SE = 1.54; $p = 3.44 \times 10^{-5}$) passed the threshold for multiple testing (see Table 2, Fig 1B).

Next, an inverse-variance-weighted meta-analysis combining all available cohorts (OPPERA discovery, TMD case control, PMPS, and CPPC) was done for a total sample size of 4,796. The SNP rs11575542 was found to be the most statistically significant hit, passing correction for multiple testing with $p = 6.43 \times 10^{-8}$ (Table 3). We then chose this SNP for further functional analysis. The nonsynonymous nature of the substitution allowed structural, cellular, and enzymatic tests.

Molecular Dynamics Simulation

DDC encodes the AADC enzyme. The name of the enzyme is L-aromatic amino acid decarboxylase, because it decarboxylates a number of amino acids, including L-dopa and tryptophan, producing dopamine and 5-HT. However, because its role in producing dopamine from L-dopa is so clinically important, it is often called dopa decarboxylase. However, a missense mutation in this gene would cause it to be unable to produce either dopamine or 5-HT. AADC is a homodimer polypeptide that is functioning as a dimer, where the dimerization surface contains electrostatic hot spots essential for catalytic site function and binding of PLP. In the holo form, the binding of the L-amino acid substrate involves global conformational changes. The SNP rs11575542 is a missense substitution that results in an arginine (R) to glutamine (Q) change at position 462 located in the C-terminal helix of the AADC protein (Fig 2A, B). Site 462 is not immediately located to the active site of AADC, but we hypothesized that it could mediate long-range allosteric control, as

found in other proteins.³⁵ Moreover, examination of the substitution position identified its potential influence on the binding of AADC PLP cofactor rather than the catalytic center. To test the impact of an R to Q substitution at position 462 on the conformational dynamics of AADC, we performed molecular dynamics simulations. We engineered the substitution into the dimeric 3-dimensional (3D) structure of the wild type, both with the PLP cofactor (holo form, PDB ID: 3RCH) and without the PLP cofactor (apo form, PDB ID: 3RBF). The apo and holo forms of both R462 and Q462 were submitted to 10-nanosecond production runs.

To quantify the effect of the substitution on protein flexibility, we calculated the backbone root-mean-square deviation (RMSD) with respect to the 3D structure at the start of the simulation (see Fig 2C, D). The RMSDs suggest that molecular dynamics simulation for all 4 systems reached equilibrium after 3 nanoseconds. The holo-R462 reached a peak RMSD of 0.563nm (5.63Å), whereas the holo-Q462 counterpart reached a peak RMSD of 0.525nm (5.25Å). This suggests that rs11575542 does not significantly affect the flexibility of the holo form. Interestingly, the apo-R462 reached a similar level of RMSD at 0.514nm (5.14Å), but the structure apo-Q462 is significantly more rigid than apo-R462, with an observed RMSD of 0.437nm. Specifically, the low RMSD observed in the apo-Q462 is due to the low number of movements made by the structure while in simulation, as apo-Q462 forms a relatively close alignment with its premolecular dynamic structure.

The role of PLP is key to direct the movement of the dimer during the simulation. The AADC dimer moves to close itself around the PLP cofactor and forms a protective shell. The ligand moves freely inside this pocket during production runs (see Fig 2). Following these simulations, we calculated the overall binding energies of AADC with PLP using *g_mmpbsa*.³⁶

TABLE 2. Association Results of 5 Candidate SNPs in 3 Replication Cohorts

SNP	EA	TMD Case-Control		PMPS		CPPC		Meta-Analysis	
		β (SE)	<i>p</i>	β (SE)	<i>p</i>	β (SE)	<i>p</i>	Effect (SE)	<i>p</i>
rs2498982	G	0.84 (0.76)	0.27	-1.48 (2.25)	0.51	-2.44 (1.77)	0.17	0.17 (0.67)	0.80
rs3765550	C	0.80 (0.77)	0.30	-1.10 (2.37)	0.64	-0.67 (1.82)	0.71	0.44 (0.68)	0.52
rs1563945	C	-0.89 (0.93)	0.34	-0.22 (3.48)	0.95	0.97 (2.71)	0.72	-0.67 (0.86)	0.44
rs11575542 ^a	T	6.62 (1.65)	6.27E-05	10.03 (8.61)	0.25	3.02 (4.86)	0.54	6.37 (1.54)	3.44E-05 ^a
rs3020422	A	0.48 (0.77)	0.53	-5.36 (2.37)	0.02	1.82 (1.86)	0.33	0.17 (0.68)	0.80

The meta-analysis refers to an inverse-variance-weighted meta-analysis of TMD case-control, PMPS, and CPPC.

^aSNP that pass $p < 1.0E-02$.

CPPC = complex persistent pain conditions cohort; EA = effect allele; PMPS = postmastectomy pain syndrome cohort; SE = standard error; SNP = single nucleotide polymorphism; TMD = temporomandibular disorders case-control cohort.

TABLE 3. Meta-Analysis of 5 Candidate SNPs Combining All Cohorts (n = 4,796)

SNP	Chr	Gene	Function	EA	Meta-Analysis	
					β (SE)	<i>p</i>
rs2498982	1	<i>PATJ</i>	Missense	G	1.34 (0.51)	8.81E-03
rs3765550	9	<i>MPDZ</i>	Intron	C	1.46 (0.53)	5.56E-03
rs1563945	8	<i>PNOG</i>	Intron	C	-1.89 (0.65)	3.79E-03
rs11575542	7	<i>DDC</i>	Missense	T	6.40 (1.18)	6.43E-08
rs3020422	6	<i>ESR1</i>	Intron	A	-1.05 (0.53)	4.62E-02

Chr = chromosome; *DDC* = L-aromatic amino acid decarboxylase; EA = effect allele; *ESR1* = estrogen receptor 1; *MPDZ* = multiple PDZ domain crumbs cell polarity complex component; *PATJ* = PatJ, crumbs cell polarity complex component; *PNOG* = prepronocceptin; SE = standard error; SNP = single nucleotide polymorphism.

Q462 has more positive binding energies of the AADC/PLP complex compared to the R462, signifying a lower binding affinity of PLP to AADC. We subsequently calculated the contribution of each active site residue to the binding energies of PLP with AADC. With Q462, active site energy contribution shifts from -11.60kJ/mol to $+18.72\text{kJ/mol}$. The main AADC residue, LYS-303, which binds to PLP via a Schiff base, has the highest energy change following Q462 mutation, going from -38.79kJ/mol to -15.09kJ/mol . Another residue involved in forming a hydrogen bond between PLP and AADC, His-192, undergoes a significant change in binding energies, adjusting from -9.48kJ/mol to -4.05kJ/mol . These 2 residues contribute significantly to the binding energy changes following R462Q mutation in AADC, whereas the other residues in the active site do not undergo significant energetic modifications. Based on these observations, we conclude that Q462 changes the binding energy of PLP with AADC by increasing its energetic demands and lowering binding affinity between the inhibitor and the target protein. The R462Q substitution renders the AADC stiffer and less flexible to receive the cofactor; ergo, the change in deviation observed for the apo-Q462 is lower than for the apo-R462 structures. Altogether, the molecular dynamics simulations demonstrate that the substitution change dramatically reduces the conformational dynamics of the AADC 3D structure, which leads to less binding capacity to its cofactor PLP. Next, we sought to verify whether the stiffness of the enzyme in the AADC_Q affects its abundance level through protein stability and/or its catalytic activity.

In Vitro Testing of AADC Variants

To understand how the nonsynonymous substitution in AADC affects its enzymatic function, we created expression vectors with major and minor alleles (*DDC_t* for mutant AADC_Q and *DDC_c* for wild-type AADC_R) and transfected human embryonic kidney cells 293 (HEK293) cells with both

constructs. We first quantified protein levels of AADC variants from transfected cell lines using Western blot. The relative expression levels of AADC_Q and AADC_R were consistently similar in both conditions. Also, HEK293 cells did not display background expression or activity that could confound the results. Another cell line, BE(2)-C neuroblastoma, had an abundance of AADC and served as a positive control for the specificity of the antibody (Fig 3A).

We next evaluated the functionality of the AADC variants with an in vitro enzymatic activity assay (see Fig 3B). Michaelis–Menten kinetics parameters were obtained from full kinetic curves using L-dopa or 5-HTP as a substrate at 0 to 1,000 μM . In both cases we observed a significant 20% to 23% reduction in the V_{max} of the AADC_Q ($F_{4,4}$; $p < 0.01$ for 5-HTP; $p < 0.05$ for L-dopa, Student unpaired *t* test). The difference between K_m values did not reach statistical significance, although the mutant AADC_Q appears to have a lower K_m . It must also be noted here that the lysate had to be diluted 1:10 for L-dopa to obtain a full kinetic curve within the same substrate range as for 5-HTP, reflecting the generally higher capacity of AADC for L-dopa to DA conversion.

From these experiments, we concluded that the minor allele does not affect the level of protein expression of AADC in vitro, but it changes the enzymatic activity of the protein. Essentially, the output capacity of AADC_Q is saturated at lower substrate concentrations in comparison to the wild-type AADC_R, which leads to lower amounts of the final product (DA or 5-HT) being produced.

Plasma Levels of 5-HT

To relate the in vitro enzymatic activity results into physiological conditions, we measured the products of AADC, namely DA and 5-HT levels, in a subgroup of 90 participants from the CPPC cohort. We were not able to detect DA in plasma, but the mean levels of 5-HT were $6.13 \pm 16.27\text{ng/ml}$. We found

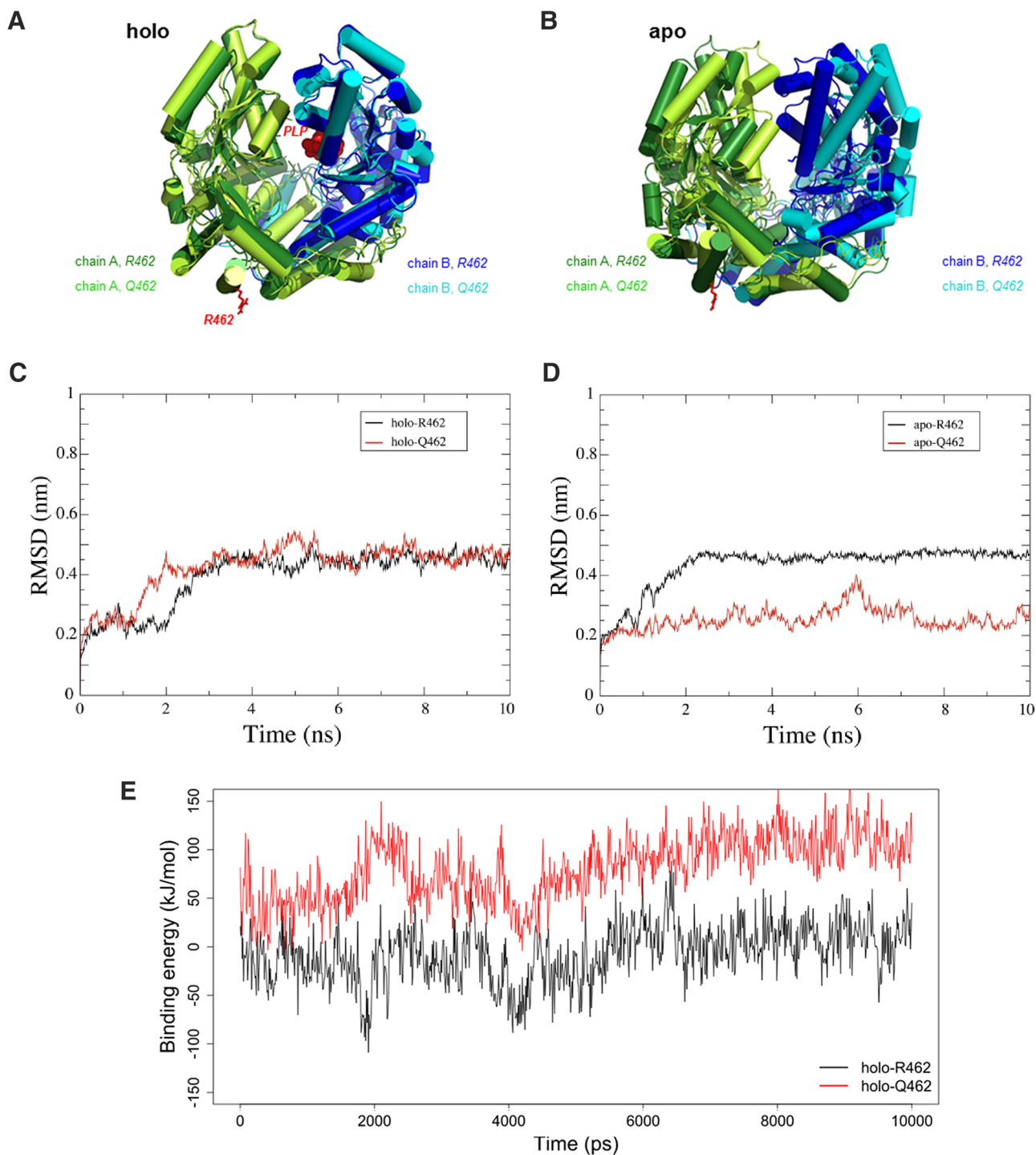


FIGURE 2: Molecular dynamics of AADC. (A) Structural alignment between the holo forms of the AADC R462 (wild type) and Q462 (substitution). Dark green and dark blue represent the dimer of the wild type. Light green and light blue represent the homodimer of the substitution. Residue R462 is shown as sticks, whereas the ligand PLP is shown as spheres. The centroid from clustered frames postmolecular dynamics simulations were used for alignment. Structural alignment was performed with PyMol. (B) Structural alignment between the apo forms of the AADC R462 and Q462. Color scheme is similar to A. (C) Effect of the substitution on the flexibility of the holo form as measured by backbone root-mean-square deviation (RMSD). RMSD was calculated with respect 3-dimensional structure at the start of the simulation (time = 0). (D) Effect of the substitution on the flexibility of the apo form. (E) Binding energies for the complete AADC/PLP complex between R462 and Q462. The majority of the simulations for Q462 are spent in a positive binding energy environment, whereas for R462 they are spent in a negative binding energy environment. AADC = L-aromatic amino acid decarboxylase; PLP = pyridoxal 5'-phosphate.

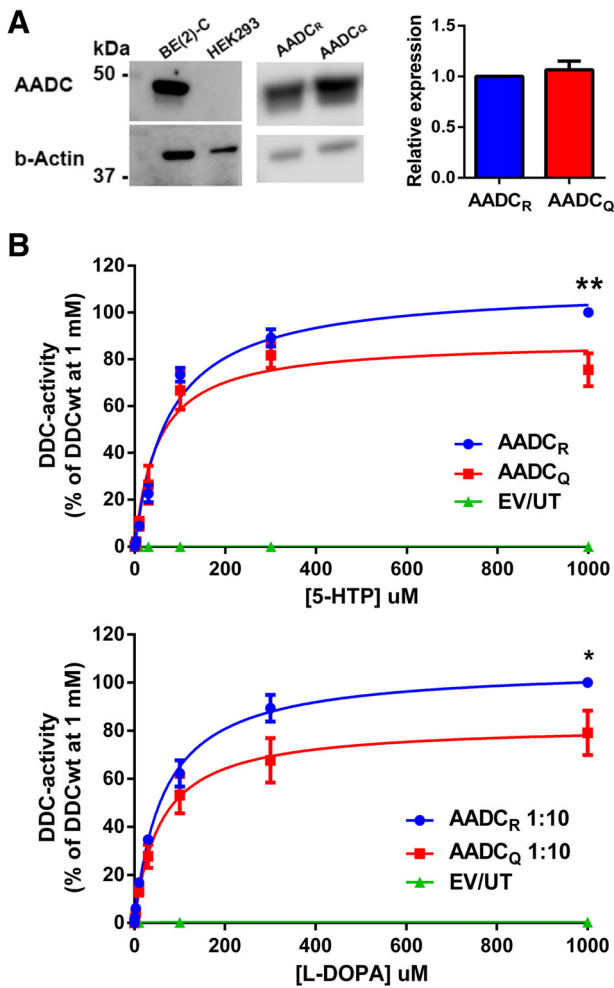


FIGURE 3: In vitro assays and enzymatic activity curves for L-aromatic amino acid decarboxylase (AADC). (A) Protein expression levels of AADC_R and AADC_Q in transfected HEK293 cells. AADC was not detected in HEK293 cells, so the antibody was validated with BE(2)-C neuroblastoma cells. Both variants were expressed at similar levels. All results are expressed as mean \pm standard error of the mean ($n = 5$). (B) Enzymatic activities of AADC_R and AADC_Q transiently expressed in HEK293 cells. Michaelis-Menten kinetics with 0 to 1,000 μ M serotonin (5-HTP) or L-dopa as a substrate; each data point is normalized to AADC_R 1,000 μ M. The maximum velocity of AADC_Q was significantly lower than that of AADC_R for both substrates (F4,4; $**p < 0.01$, $*p < 0.05$; Student unpaired t test). Results are expressed as mean \pm standard error of the mean ($n = 5$). AADC_Q = L-aromatic amino acid decarboxylase for glutamine; AADC_R = L-aromatic amino acid decarboxylase for arginine; EV/UT = Empty vector / Untransfected. [Color figure can be viewed at www.annalsofneurology.org]

a negative correlation between plasma levels of 5-HT and PILL global scores (Spearman $\rho = -0.272$; $p = 1.2 \times 10^{-2}$); participants with worse somatic symptoms have lower 5-HT plasma levels (Fig 4A). To ensure this correlation was not due to participants' medication use, we evaluated if any participants were taking SSRIs. Out of the 90 participants from the CPPC cohort who were assessed for 5-HT plasma levels, 13 participants were

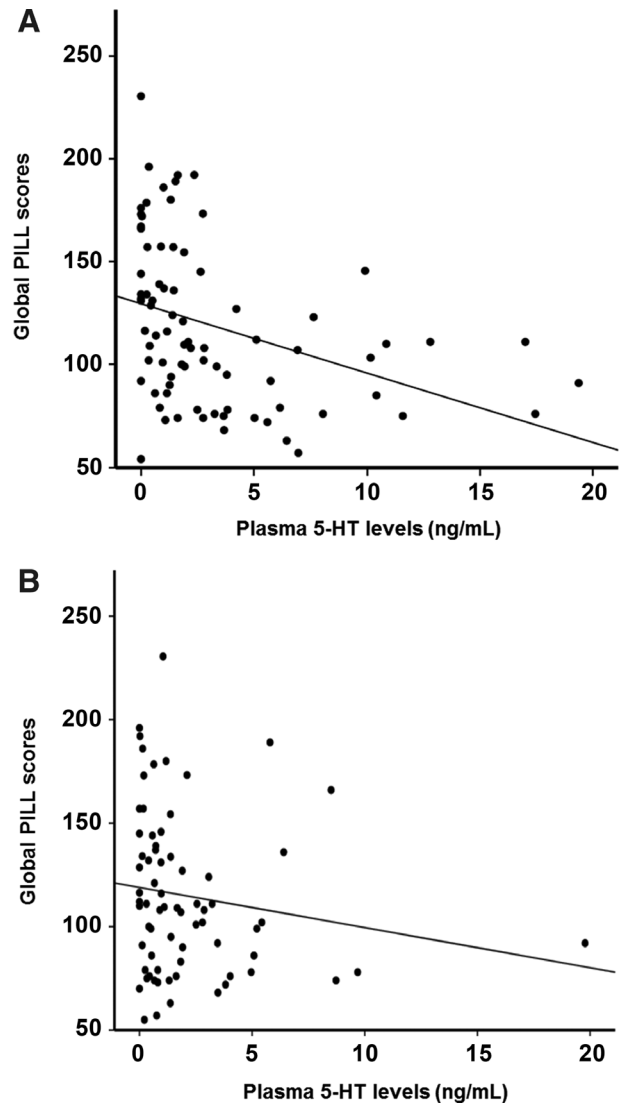


FIGURE 4: Correlation plot between plasma serotonin (5-HT) levels and Pennebaker Inventory of Limbic Languidness (PILL) questionnaire global scores. (A) Scatter plot between PILL global scores and 5-HT plasma levels in 90 individuals from the complex persistent pain conditions (CPPC) cohort. (B) Scatter plot between PILL questionnaire global scores and 5-HT plasma levels in 77 individuals from the CPPC cohort, excluding individuals taking selective serotonin reuptake inhibitors.

taking SSRIs. We then took further steps and tested the mean difference in PILL scores and in 5-HT plasma levels in subjects taking SSRIs versus subjects not taking SSRIs. We found no statistically significant difference in either PILL scores or 5-HT levels. Those taking SSRIs had slightly higher PILL global scores than those not taking SSRIs (129.9 ± 43.7 vs 114.4 ± 38.8 ; $p = 0.21$). Those taking SSRIs had lower 5-HT plasma levels than those not taking SSRIs (1.05 ± 1.3 vs 6.98 ± 17.5 , $p = 0.22$). When we excluded participants taking SSRIs, the original correlation between plasma levels of 5-HT and PILL global scores remained statistically significant (Spearman $\rho = -0.237$; $p = 0.045$).

Even though chronic TMD cases report more somatic symptoms than healthy controls, rs11575542 in *DDC* was not associated with TMD case status, and there was no difference in 5-HT plasma levels in TMD cases versus controls (data not shown).

Discussion

Persistent somatic symptoms are debilitating to patients and are a source of distress. Our study provides new insight into the pathophysiology of somatic symptoms and suggests an identifiable physiological mechanism that underlies the manifestation of these symptoms. In turn, these results open the door to evidence-based treatment options that target the serotonergic system in patients with high level of somatic symptoms.

In this study, we sought to identify genetic polymorphisms that contribute to heightened frequency of somatic symptoms to start to build our understanding of molecular pathophysiology of this psychological trait. We found that the minor allele of rs11575542, located in the *DDC* gene, is associated with a greater frequency of somatic symptoms. Although the frequency of the minor allele for rs11575542 is not very high, the effect of the allele is not recessive but codominant. Thus, almost 10% of the population, including both homozygotes and heterozygotes, will be affected by this allele. Furthermore, the value of our results is beyond the identification of a particular functional allele. Our results identified the first molecular pathway underlying somatic symptoms reporting. This SNP was not previously associated at a genome-wide level with any phenotype. With more cohorts being collected relevant to somatic awareness, we hope to see further associations.

The minor T allele of rs11575542 codes for an enzyme variant that replaces an arginine to a glutamine at position 462 close to the C-terminus in the AADC protein. Our molecular dynamic simulation suggested that this change makes the enzyme less flexible and renders it less effective to binding its cofactor PLP. In an enzymatic assay, we showed that R462Q substitution reduces the maximum kinetic velocity of AADC and hence reduces the production of 5-HT and DA. Consistent with our in vitro analysis results, we demonstrated that reduced plasma levels of 5-HT are correlated with an enhanced frequency of somatic symptoms.

The *DDC* gene is located on chromosome 7 and spans more than 85kb. It is composed of 15 exons, and alternative splicing confers tissue-specific expression of the enzyme AADC.³⁷ AADC is a PLP-dependent enzyme belonging to group II,³⁸ and shares structural similarities with other decarboxylases.³⁹ The principal role of AADC is to supply the organism with essential neurotransmitters by contributing to their synthesis through the decarboxylation reactions and therefore control aromatic amine levels.⁴⁰ In normal DA and

5-HT neurotransmitter synthesis, AADC is not the rate-limiting step in either reaction⁴¹; however, in our association analysis it was clearly correlated with 5-HT level. This finding suggests that in normal physiological conditions AADC still contributes substantially to the 5-HT and possibly dopamine levels. Furthermore, in humans, AADC is the rate-limiting enzyme in the formation of trace amines,⁴² which also plays a critical role in pain pathways and can be considered for further analysis for its potential contribution to somatization.

AADC is widely expressed in the central nervous system.⁴³ We, however, used HEK293 kidney cells in our enzymatic assays because the intention of the in vitro assays was not to mimic the full DA/5-HT pathways. Our goal was merely a production of AADC allelic variants via transient transfection for measuring its allele-dependent enzymatic activity. HEK293 cells lack native AADC expression, so all AADC activity in the samples was derived from our constructs. However, to understand the physiological role of AADC in the DA/5-HT synthetic pathways sufficiently, further experiments should be done in neuronal cells.

Loss of function mutations in *DDC* have previously been described in an inherited disorder termed AADC deficiency. This disease is very severe, with symptoms of infantile Parkinsonism and developmental delay, usually leading to death. Another set of symptoms of this disorder affect the autonomic dysfunctions with symptoms including sweating, nasal congestion, hypoglycemia, and acid reflux that are also captured by the PILL questionnaire, but certainly to a much milder extent.⁴⁴ A mouse model of a more mildly pathogenic AADC deficiency, the S250F mutation (rs137853208), has been created, and the mutant mouse displays a substantially reduced enzymatic activity of AADC. This led to a modest reduction of DA in the brain but a large decrease of 5-HT. Analogous to the results that we report, authors found similar levels of the protein expressed in wild-type and mutated *DDC*. The resulting phenotype of the mutant mice was serotonergic in nature, affecting temperature and autonomic functions.⁴⁵ Whether the effect that we are observing in clinical samples is due to a peripheral or central effect of AADC is unknown.

As of yet, there are no animal assays to study somatic symptoms in spite of the importance of these endophenotypes in chronic pain states and other clinical conditions. The lack of animal assays is partly due to the lack of mechanistic understanding on the neurobiology of somatic symptoms. Our results would allow developing such assays that can be used to study systemic pathophysiology of somatization phenotypes and provide the means for treatment development.

It was previously shown that SSRIs are efficacious against somatic symptoms disorders^{46–48}; however, their efficacy was attributed to an analgesic effect. Our results

suggest that their therapeutic effect might not be through analgesic effect but rather direct alleviation of somatic symptoms. In the field of depression, some studies propose that patients with somatic manifestation of depression, such as the presence of gastrointestinal symptoms, can be treated by SSRIs.^{49,50} The same is true for fibromyalgia, where treatment with SSRIs improves somatic symptoms.⁵¹ Our results suggest a mechanism for this reported efficacy of SSRIs.

This study presents major limitations that should be addressed. First, we used a candidate gene panel and not a genome-wide approach to search for genetic association with the PILL. Although a candidate gene panel limits the possibility of discovery, a well-curated, broad gene panel can look for pathological processes in modestly sized cohorts by focusing on a limited number of pathways with higher relevance. Pathways assessed by the gene panel used in this study represent 1 or more of 3 broad domains of pain perception, inflammatory response, and mood and affective disorders. All of these domains are known to overlap with somatic symptoms. Furthermore, the SNPs were chosen based on potential functionality and previous evidence for associations with related phenotypes. Therefore, by using a well-curated SNP list, we targeted our search to pursue a functional genomics study. Furthermore, in a recently published article, we demonstrated that reproducibility rates of candidate SNPs in independent cohorts are comparable to those from genome-wide association studies⁵² and thus are reliable for use in targeted functional genomics studies. Finally, and more importantly, in a combined meta-analysis of all 4 available cohorts, our association with rs11575542 reached strong statistical significance ($p = 6.43 \times 10^{-8}$).

In summary and based on our results, we suggest that rather than viewing somatoform disorders as a psychiatric issue, physical symptom reporting that underlies the somatoform disorders should be considered as a pathophysiological condition in which physical and psychological manifestations have a common molecular biochemical origin acting through a serotonergic mechanism. We describe a molecular mechanism by which a minor allele in AADC lowers 5-HT plasma levels and thus possibly contributes to the emergence of somatic symptoms. Targeting somatic symptoms by increasing the levels of 5-HT using SSRIs, for example, should be tested in individuals with high somatic scores, and carriers of the minor allele of rs11575542 can be hypothesized to display the best response.

Acknowledgment

This work was supported by the Canadian Institutes of Health Research (G237818/CERC09/CIHR to L.D.),

Natural Sciences and Engineering Research Council of Canada (to A.S.), and NIH National Institute of Dental and Craniofacial Research grant U01DE017018. A.-T.T. acknowledges a fellowship from the University of Montreal Faculty of Graduate and Postdoctoral Studies.

Author Contributions

S.K., S.B.S., I.B., G.D.S., R.B.F., J.D.G., R.O., W.M., and L.D. contributed to the conception and design of the study. S.K., M.H.P., A.-T.T., T.C., A.S., G.G.N., and A.W.R.S. contributed to the acquisition and analysis of data. S.K., M.H.P., A.-T.T., and L.D. contributed to the drafting of the text and preparing the figures.

Potential Conflicts of Interest

Nothing to report.

References

1. Barsky AJ. Assessing the new DSM-5 diagnosis of somatic symptom disorder. *Psychosom Med* 2016;78:2–4.
2. Reynolds E, Ward L. Somatic awareness and symptom attribution in ischemic stroke patients. *J Neurosci Nurs* 2014;46:5–62.
3. Rief W, Broadbent E. Explaining medically unexplained symptoms—models and mechanisms. *Clin Psychol Rev* 2007;27:821–841.
4. Escobar JI, Manu P, Matthews D, et al. Medically unexplained physical symptoms, somatization disorder and abridged somatization: studies with the Diagnostic Interview Schedule. *Psychiatr Dev* 1989; 7:235–245.
5. Katon W, Lin E, Von Korff M, et al. Somatization: a spectrum of severity. *Am J Psychiatry* 1991;148:34–40.
6. O'Brien EM, Atchison JW, Gremillion HA, et al. Somatic focus/awareness: relationship to negative affect and pain in chronic pain patients. *Eur J Pain* 2008;12:104–115.
7. von Korff M, Dworkin SF, LeResche L, Kruger A. An epidemiological comparison of pain complaints. *Pain* 1988;32:173–183.
8. McCracken LM, Faber SD, Janeck AS. Pain-related anxiety predicts non-specific physical complaints in persons with chronic pain. *Behav Res Ther* 1998;36:621–630.
9. Dworkin SF, Von Korff M, LeResche L. Multiple pains and psychiatric disturbance. An epidemiological investigation. *Arch Gen Psychiatry* 1990;47:239–244.
10. Manfredini D, Winocur E, Ahlberg J, et al. Psychosocial impairment in temporomandibular disorders patients. RDC/TMD axis II findings from a multicentre study. *J Dent* 2010;38:765–772.
11. Fillingim RB, Ohrbach R, Greenspan JD, et al. Potential psychosocial risk factors for chronic TMD: descriptive data and empirically identified domains from the OPPERA case-control study. *J Pain* 2011;12: T46–T60.
12. Wolfe F, Walitt BT, Katz RS, Hauser W. Symptoms, the nature of fibromyalgia, and diagnostic and statistical manual 5 (DSM-5) defined mental illness in patients with rheumatoid arthritis and fibromyalgia. *PLoS One* 2014;9:e88740.
13. Fillingim RB, Ohrbach R, Greenspan JD, et al. Psychological factors associated with development of TMD: the OPPERA prospective cohort. *J Pain* 2013;14:T75–T90.
14. Pennebaker JW. *The Psychology of Physical Symptoms*. New York, NY: Springer-Verlag, 1982.

15. Maixner W, Diatchenko L, Dubner R, et al. Orofacial pain prospective evaluation and risk assessment study—the OPPERA study. *J Pain* 2011;12:T4–T11.
16. Smith SB, Maixner DW, Greenspan JD, et al. Potential genetic risk factors for chronic TMD: genetic associations from the OPPERA case control study. *J Pain* 2011;12:T92–T101.
17. Slade GD, Bair E, By K, et al. Study methods, recruitment, sociodemographic findings, and demographic representativeness in the OPPERA study. *J Pain* 2011;12:T12–T26.
18. Pennebaker JW. Putting stress into words: health, linguistic and therapeutic implications. *Behav Res Ther* 1993;31:539–548.
19. Purcell S, Neale B, Todd-Brown K, et al. PLINK: a tool set for whole-genome association and population-based linkage analyses. *Am J Hum Genet* 2007;81:559–575.
20. Slade GD, Smith SB, Zaykin DV, et al. Facial pain with localized and widespread manifestations: separate pathways of vulnerability. *Pain* 2013;154:2335–2343.
21. Belfer I, Schreiber KL, Shaffer JR, et al. Persistent postmastectomy pain in breast cancer survivors: analysis of clinical, demographic, and psychosocial factors. *J Pain* 2013;14:1185–1195.
22. Willer CJ, Li Y, Abecasis GR. METAL: fast and efficient meta-analysis of genomewide association scans. *Bioinformatics* 2010;26:2190–2191.
23. Giardina G, Montioli R, Gianni S, et al. Open conformation of human DOPA decarboxylase reveals the mechanism of PLP addition to Group II decarboxylases. *Proc Natl Acad Sci U S A* 2011;108:20514–20519.
24. Yin S, Ding F, Dokholyan NV. Eris: an automated estimator of protein stability. *Nat Methods* 2007;4:466–467.
25. Abraham MJ, Murtola T, Schulz R, et al. GROMACS: high performance molecular simulations through multi-level parallelism from laptops to supercomputers. *SoftwareX* 2015;1–2:19–25.
26. Schmid N, Eichenberger AP, Choutko A, et al. Definition and testing of the GROMOS force-field versions 54A7 and 54B7. *Eur Biophys J* 2011;40:843–856.
27. Schüttelkopf AW, van Aalten DMF. PRODRG: a tool for high-throughput crystallography of protein-ligand complexes. *Acta Crystallogr* 2004;D60:1355–1363.
28. Berendsen HJ, Grigera JR, Straatsma TP. The missing term in effective pair potentials. *J Physical Chem* 1987;91:6269–6271.
29. Essmann U, Perera L, Berkowitz ML et al. A smooth particle mesh Ewald method. *J Chem Physics* 1995;103:8577.
30. Bussi G, Donadio D, Parrinello M. Canonical sampling through velocity rescaling. *J Chem Physics* 2007;126:014101.
31. Parrinello M. Polymorphic transitions in single crystals: a new molecular dynamics method. *J Appl Phys* 1981;52:7182.
32. Hess B, Bekker H, Berendsen HJ, Fraaije JG. LINCS: a linear constraint solver for molecular simulations. *J Comput Chem* 1997;18:1463–1472.
33. Humphrey W, Dalke A, Schulten K. VMD: visual molecular dynamics. *J Mol Graph* 1996;14:33–38.
34. Allen GFG. *The neurochemical consequences of aromatic l-amino acid decarboxylase deficiency [dissertation]*. London, UK: University College London, 2010.
35. Dokholyan NV. Controlling allosteric networks in proteins. *Chem Rev* 2016;116:6463–6487.
36. Kumari R, Kumar R, Lynn A. g_mmpbsa—a GROMACS tool for high-throughput MM-PBSA calculations. *J Chem Inf Model* 2014;54:1951–1962.
37. Sumi-Ichinose C, Ichinose H, Takahashi E, et al. Molecular cloning of genomic DNA and chromosomal assignment of the gene for human aromatic L-amino acid decarboxylase, the enzyme for catecholamine and serotonin biosynthesis. *Biochemistry* 1992;31:2229–2238.
38. Percudani R, Peracchi A. A genomic overview of pyridoxal-phosphate-dependent enzymes. *EMBO Rep* 2003;4:850–854.
39. Sanchez-Jimenez F, Pino-Angeles A, Rodriguez-Lopez R, et al. Structural and functional analogies and differences between histidine decarboxylase and aromatic l-amino acid decarboxylase molecular networks: biomedical implications. *Pharmacol Res* 2016;114:90–102.
40. Bertoldi M. Mammalian dopa decarboxylase: structure, catalytic activity and inhibition. *Arch Biochem Biophys* 2014;546:1–7.
41. Berry MD, Juorio AV, Li XM, Boulton AA. Aromatic L-amino acid decarboxylase: a neglected and misunderstood enzyme. *Neurochem Res* 1996;21:1075–1087.
42. Scherer LJ, McPherson JD, Wasmuth JJ, Marsh JL. Human dopa decarboxylase: localization to human chromosome 7p11 and characterization of hepatic cDNAs. *Genomics* 1992;13:469–471.
43. Ren LQ, Chen M, Hultborn H, et al. Heterogenic distribution of aromatic L-amino acid decarboxylase neurons in the rat spinal cord. *Front Integr Neurosci* 2017;11:31.
44. Brun L, Ngu LH, Keng WT, et al. Clinical and biochemical features of aromatic L-amino acid decarboxylase deficiency. *Neurology* 2010;75:64–71.
45. Caine C, Shohat M, Kim JK, et al. A pathogenic S250F missense mutation results in a mouse model of mild aromatic l-amino acid decarboxylase (AADC) deficiency. *Hum Mol Genet* 2017;26:4406–4415.
46. Somashekar B, Jainer A, Wuntakal B. Psychopharmacotherapy of somatic symptoms disorders. *Int Rev Psychiatry* 2013;25:107–115.
47. Kroenke K. Efficacy of treatment for somatoform disorders: a review of randomized controlled trials. *Psychosom Med* 2007;69:881–888.
48. Sussman N. SNRIs versus SSRIs: mechanisms of action in treating depressions and painful physical symptoms. *Prim Care Companion J Clin Psychiatry* 2003;5:19–26.
49. De Wester JN. Recognizing and treating the patient with somatic manifestations of depression. *J Fam Pract* 1996;43:S3–S15.
50. Linden RD, Wilcox CS, Heiser JF, et al. Are selective serotonin reuptake inhibitors well tolerated in somatizing depressives? *Psychopharmacol Bull* 1994;30:151–156.
51. Rao SG, Bennett RM. Pharmacological therapies in fibromyalgia. *Best Pract Res Clin Rheumatol* 2003;17:611–627.
52. Meloto CB, Benavides R, Lichtenwalter RN, et al. Human pain genetics database: a resource dedicated to human pain genetics research. *Pain* 2018;159:749–763.